analytical chemistry

Article

pubs.acs.org/ac

Lithium Ion Quantification Using Mercury Amalgams as *in Situ* Electrochemical Probes in Nonaqueous Media

Zachary J. Barton and Joaquín Rodríguez-López*

Department of Chemistry, University of Illinois at Urbana−Champaign, 58 Roger Adams Laboratory, 600 South Matthews Avenue, Urbana, Illinois 61801, United States

Supporting Information

ABSTRACT: We report on the quantitative, spatially resolved study of ionic processes for energy materials in nonaqueous environments by *in situ* electrochemical means at the micro- and nanoscale. Mercury-capped platinum ultramicroelectrodes (Hg/Pt UMEs) were tested as probes for alkali ions in propylene carbonate (PC) in an oxygen- and water-free environment. Anodic stripping voltammetry (ASV) performed at Hg/Pt UMEs displayed a linear response to Li^+ concentration extending from 20 μM to at least 5 mM. The sensitivities of these probes for ionic lithium are 1.93 and −23.2 pA μM^{-1} by the steady-state amalgamation current and the peak stripping current, respectively. These values showed excellent agreement with simulated results as well as to those obtained experimentally for Cd^{2+} in H_2O. We further explored the interfacial imaging of lithium ion flux at an electrified interface. Scanning electrochemical microscopy (SECM) using Hg/Pt UMEs showed that the steady-state amalgamation of ionic lithium could be used to reliably position a probe close to a substrate. Investigations on a selectively insulated gold electrode in an organic solvent system showcased the response of Hg/Pt UMEs to lithium uptake by an electroactive material. Additionally, lithium stripping voltammetry at Hg deposits on a 120 nm carbon nanoelectrode demonstrated the possibility of implementing the introduced imaging strategy at the nanoscale. This work opens a way to directly correlate material defects and reactive heterogeneity in energy materials with unprecedented spatial and temporal resolution.

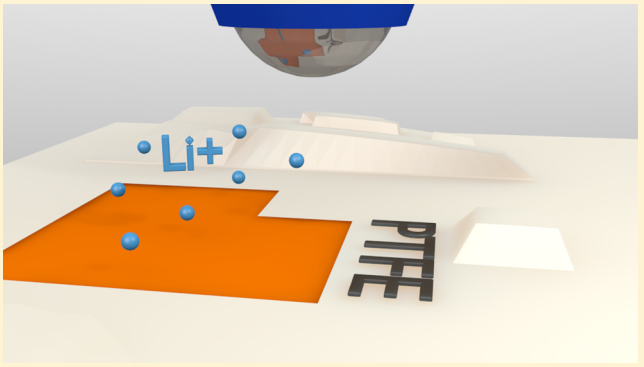

Charge transfer across the interface between an electrode and an electrolyte solution involves both electronic and ionic components. Although many aspects of bulk ionic transport in electrochemical cells are well understood,[1−3] the interfacial dynamics of ions in ion-batteries,[4−8] nanoporous separation membranes,[9] and supercapacitors,[10] systems that rely on *heterogeneous* ion transfer, have yet to be elucidated. Progress on this front has been hampered by the paucity of quantitative techniques for detecting interfacial ion fluxes of alkali metals such as Li^+, Na^+, and K^+ in nonaqueous environments.[4,8]

Recent interest in the imaging of electrochemical energy materials in nonaqueous media has fostered the development of different strategies for the localized detection of alkali ion fluxes. Among them are electrochemical strain microscopy (ESM),[11] scanning ion conductance microscopy (SICM),[12,13] and scanning electrochemical microscopy (SECM) approaches that employ solvent decomposition[14] or mediator competition[15] as indirect chemical probes. Alternative ion-sensitive techniques such as those based on the ion transfer across liquid−liquid interfaces[16−19] have also showed promise but seem challenging to implement for alkali ions in nonaqueous media. Most recently, lithium intercalation events have been resolved on the nanoscale in aqueous conditions by coupling an electrochemical thin layer flow cell to a transmission electron microscope (TEM).[20] Each of these approaches has much to recommend it but lacks sufficient chemical specificity or chemo-physical stability to adequately address questions presently facing energy material research.[8,10]

SECM is an emerging technique for probing the *in situ* dynamics of electrochemical energy systems.[21−26] Following our interest in electrode heterogeneity studied by SECM,[27,28] we introduce here an approach for the imaging and quantification of Li^+ flux at an electrified interface in an organic medium. By monitoring electrochemical ion-reduction and stripping reactions at Hg-capped Pt ultramicroelectrodes (UMEs), we also demonstrate the feasibility of our approach for the simultaneous analysis of multiple alkali ions and for its application at the nanoscale.

In aqueous media, Hg-based probes have demonstrated mechanical stability,[29] chemical specificity on the basis of reduction potentials and stripping traits,[30] and reliable current response to rapid changes in potential and ion flux.[31] They also have an unmatched distinction among analogous probes for circumventing competing processes, such as solvent decom-

Received: July 9, 2014
Accepted: October 13, 2014
Published: October 13, 2014

   dx.doi.org/10.1021/ac502517b | *Anal. Chem.* 2014, 86, 10660−10667

position reactions at highly reducing potentials.[32,33] When coupled to SECM, Hg probes facilitate metal-selective reactive imaging.[34] Also, the further incorporation of fast-scan anodic stripping voltammetry (ASV) has allowed rapid, microresolved interrogations of the electrodeposition and surface corrosion of transition metals in aqueous media over regions measuring hundreds of micrometers on a side.[35,36] In these studies, the ability to controllably concentrate metals in the mercury phase facilitated their quantification from even the most dilute environments, such as near an ion-depleted surface. However, SECMs equipped with Hg-capped probes have never before been used to study Li^+.

Amalgams of lithium and other alkali metals have been studied in diverse media for nearly a century, and the resulting wealth of physical and chemical data[37−40] has enabled our investigation of lithium amalgams to be quantitative. For example, the solubility of alkali amalgams is high and in the case of Li^+ up to 1.33 mol % (898 mM),[39] which allows operation of Hg/Pt UMEs in fairly concentrated solutions without risking distortion from saturation. Additionally, studies of lithium amalgam dynamics[41,42] determined that the apparent rate constant describing the formation of Li(Hg) from Li^+ in solution can be adjusted by over 7 orders of magnitude, between 9×10^{-9} and 0.15 $cm \cdot s^{-1}$, by changing the identities of the solvent and the supporting electrolyte. For solvents commonly used in battery electrodes, e.g., propylene carbonate (PC), this reaction is fast. Armed with solubilities, rate constants, transfer coefficients, and diffusion coefficients, we here extend the application of Hg-capped UMEs to the imaging of alkali ion concentrations at electrified surfaces in organic media for resolving heterogeneous ion-coupled mechanisms in functional energy materials.

MATERIALS AND METHODS

Chemicals. Cadmium (Stick, ≥99.999%), phosphoric acid (85%), and potassium perchlorate (99%) were obtained from Alfa Aesar. Acetone, isopropanol, nitric acid, and water (ChromAr grade) were obtained from Avantor. Mercury (Quadruple distilled, 99.9999%) was obtained from Bethlehem Apparatus Co. Potassium phosphate monobasic (99.5%) were obtained from Fisher Scientific. Agar (Bacteriological grade) was obtained from Gibco. Platinum wire (25 μm and 1 mm diameter) and silver wire (1 mm diameter) were obtained from Goodfellow. Acetonitrile (MeCN), cadmium nitrate tetrahydrate, ethyl viologen diperchlorate (98%), ferrocene methanol (FcMeOH, 97%), lithium perchlorate (dry, 99.99% trace metals basis), mercury(II) nitrate monohydrate, polytetrafluoroethylene solution (PTFE, 60 wt % in H_2O), potassium nitrate (≥99%), potassium phosphate dibasic (≥98.0%), propylene carbonate (PC, anhydrous, 99.7%), sodium perchlorate (≥98%), tetrabutylammonium hexafluorophosphate (≥99.0%), tetrabutylammonium perchlorate (TBAP, ≥99.0%), and *N,N,N′,N′*-tetramethyl-*p*-phenylenediamine (TMPPD, 99%) were obtained from Sigma-Aldrich. Acetylene and ultrahigh purity argon were obtained from S. J. Smith. Undoped silicon wafers were obtained from University Wafer. All chemicals were purchased as A.C.S. reagent grade or better and used as received without further purification. The only exception to this was the metallic mercury, which was scrubbed with concentrated nitric acid before use in order to remove adventitious impurities.

Electrode Fabrication. The fabrication of metal UMEs is delineated elsewhere.[43−45] Briefly, a 25 μm diameter Pt wire was sealed inside a glass capillary with a heated metal coil, connected to a copper−tin lead with silver epoxy (Ted Pella), and then polished with 50 nm alumina particles (CHI) over a microfelt polishing pad. Before polishing, glass at the electrode's apex was removed by sharpening over silicon carbide sandpaper such that the glass-to-electrode ratio, RG = r_{Total}/r_{Pt}, was approximately 5. The oxidation of FcMeOH (Figure S-1A in the Supporting Information) served as a measure of electrode size and smoothness.

Hg was deposited on Pt UMEs from an aqueous solution of 10 mM $Hg(NO_3)_2 \cdot H_2O$, 0.1 M KNO_3, and 0.5 vol % HNO_3 as described elsewhere.[31,46,47] After confirming the electrode's cleanliness via linear sweep voltammetry (LSV) (Figure S-1B in the Supporting Information), the deposition process was accomplished by poising the working electrode at −0.1 V (vs Ag/AgCl) for 400 s in a chronoamperometric step (Figure S-1C in the Supporting Information). At the 95% confidence level, the mean charge deposited was 61 ± 12 μC, indicating that the mean Hg cap mass was 63 ± 13 ng. Optical micrographs of fabricated electrodes are available as Figure S-2 in the Supporting Information.

Nanoelectrodes. Preliminary experiments at the nanoscale were performed with Hg-capped carbon nanoelectrodes. A full description of the experimental procedure for making these nanoelectrodes will follow soon from this laboratory, building from a wealth of experimental procedures described in other works.[48−54] Briefly, quartz capillaries (o.d. = 1.0 mm, i.d. = 0.7 mm, Sutter) were pulled on a CO_2 laser-powered puller (Sutter) to yield nanopipets. Acetylene was flowed through the pipets at ∼1000 °C to yield carbon deposits. Electrodes were then characterized in 6 mM TMPPD in 0.2 M tetrabutylammonium hexafluorophosphate in MeCN. Hg deposition was carried out in a manner similar to that used for Pt UMEs.

Electrochemical Characterization. Hg-capped UMEs were used in a three-electrode configuration for alkali ion concentration dependence studies. All nonaqueous experiments of this type were performed in an argon-filled drybox (UniLab, MBraun) with a Pt wire CE placed in the same compartment as the WE and using a separate compartment for a cadmium amalgam reference (Cd^{2+}/Cd(Hg), CAR, −0.3515 V vs NHE)[3] electrode. The construction and stability of the CAR in organic solvent systems are well documented.[55−58] Though the CAR typically employs $CdCl_2$ and NaCl in conjunction, the present study instead used the nitrate salt of cadmium for its high solubility in PC. Unless otherwise stated, the electrolyte consisted of 100 mM TBAP in PC. Alkali ion spikes were added from 1000× concentrated solutions of the appropriate perchlorate salt dissolved in PC. Full calibration curves using separately prepared Hg-capped UMEs were repeated independently six times. The amalgamation and stripping currents were averaged and fit by a linear model to assess the sensitivity and limit of detection (LOD) of the probes.

For the purpose of comparison, the same W-cell was constructed in ambient conditions with 10 mM KNO_3 dissolved in H_2O, and Cd^{2+} stripping experiments were carried out using concentrations between 1 nM and 0.1 mM. Ambient ASV work and electrode fabrication was carried out with a CHI 660 potentiostat. All experiments involving lithium were performed with a SECM 420D workstation (CHI).

Nanoscale Hg electrodes were tested in a solution of PC containing 1 mM $LiClO_4$ without additional supporting electrolyte. CV was performed with the potential paused at

dx.doi.org/10.1021/ac502517b | Anal. Chem. 2014, 86, 10660−10667

−3.2 V (vs Pt QRE) at the end of the cathodic sweep for 20 s before continuing with the anodic return sweep.

SECM in Redox Competition Mode. A Au-sputtered silicon wafer was selectively insulated with a thin PTFE coat, the procedure for which is described elsewhere.[59] The initial approach of a Hg/Pt UME to a PTFE-coated area of the substrate (Figure S-8 in the Supporting Information) was performed in the feedback mode in PC containing 5.00 mM ethyl viologen diperchlorate as the redox mediator. The probe-approach curve was fit with an established mathematical model for sphere-cap electrodes[60] to obtain a tip−substrate separation of 26.2 μm (2.3·r_{Pt}). The model and fitting parameters can be found in Table S-2 in the Supporting Information. An electroactive region of bare Au was located and imaged in positive feedback mode (Figure 3). Having identified a region of interest, the cell was thoroughly rinsed and then filled with 1 mM $LiClO_4$ in PC. All SECM approach curves and images were collected with a Ag QRE to minimize crowding in the electrochemical cell. All associated potentials have been reported vs CAR for consistency by matching Li stripping potentials. With the tip poised at −2.7 V (vs CAR), the collection of Li^+ by the probe was used as the feedback mechanism to facilitate its approach to the substrate.

When near the substrate, a CV was run at the substrate with the tip held at −2.7 V (vs CAR) to verify that the amalgamation current (i_{Amal}) was sensitive to Li^+ uptake at the substrate (Figure 4B). To better visualize the competition between the substrate and the tip, CVs were also run at the tip with the substrate biased at different potentials (Figure 4C).

Digital Simulations. Simulations of binary Li amalgams were performed with a COMSOL Multiphysics model that is summarized in detail in the Supporting Information. In short, we simulated a Hg droplet suspended at an SECM tip with dimensions representative of experimental values. Electrode reactions were modeled on Butler−Volmer kinetics, and a triangular potential waveform was applied as is done in CV. The currents resulting from the amalgamation and stripping processes as well as the charge passed during stripping were compared to those obtained experimentally. All of the parameters required for simulating the studied systems were taken from the literature and are reported in Table S-1 in the Supporting Information.[39,61−65]

RESULTS AND DISCUSSION

Chemical Selectivity. Although the simultaneous reduction of alkali ions in PC requires a cathodic excursion to very reducing potentials, Hg/Pt UMEs do not sacrifice the chemical specificity that typifies stripping voltammetry. For example, Li^+ and Na^+ can be simultaneously quantified from the stripping current each produces. A CV experiment at 100 mV·s^{-1} in PC containing 150 μM Li^+, 200 μM Na^+, and 100 mM TBAP demonstrates clear stripping peak separation (Figure 1A).

While the cathodic current corresponding to the amalgamation of the two alkali ions (Figure 1A) cannot easily distinguish their relative contributions, the stripping portion of the CV is better able to resolve them. Thus, while the steady-state amalgamation of ions can be used for the total quantification of alkali ions, the stripping signal can be used to provide chemical specificity. This makes it also possible to analyze for K^+ in the presence of either Li^+ or Na^+ (Figure S-3 in the Supporting Information). We now focus on the ability of Hg-capped electrodes to quantitatively detect the most reducing metal in the alkali family: Li.

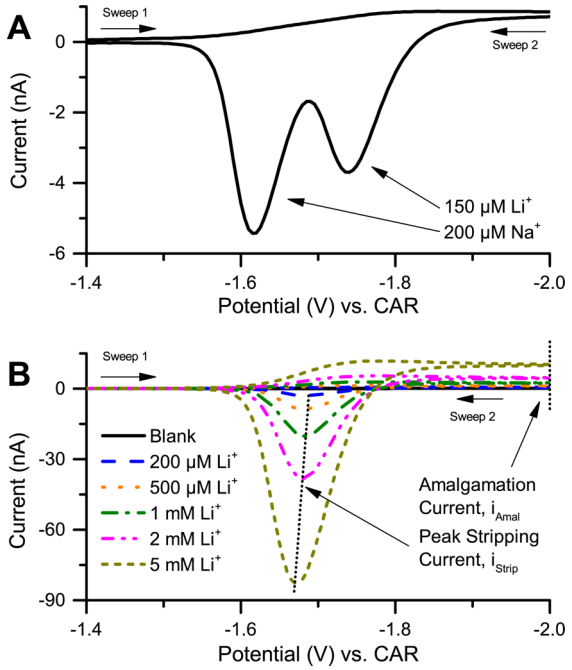

Figure 1. Stripping voltammetry of alkali ions in PC by Hg-capped Pt UMEs. (A) Experimental CV of 150 μM Li^+, 200 μM Na^+, and 100 mM TBAP in PC. The current is offset by −400 pA to account for background current. (B) Representative CVs of $LiClO_4$ and 100 mM TBAP in PC. All ν = 100 mV·s^{-1}.

Sensitivity. Pursuant to characterizing the sensitivity and LOD of Hg/Pt UMEs for Li, CV was performed in solutions of 100 mM TBAP in PC spiked with $LiClO_4$ over the range of 1−5 mM. The resulting voltammograms (Figure 1B) display a monotonic increase of both i_{Amal} (Figure 2A) and i_{Strip} (Figure 2B) as the solution ion concentration increases. The averaged results of six independent calibration curve measurements carried out with different Hg deposits in individually prepared W-cells are shown in Figure 2. A similar plot for the stripping charge is provided as Figure S-4 in the Supporting Information. The linear relationships (Table 1) derived from these concentration studies over a range of 20 μM to 5 mM allow the extrapolation of ion fluxes from measurements of current in SECM images. As expected, the preconcentration of analyte by amalgamation gives i_{Strip} a substantially higher sensitivity to changes in concentration than otherwise obtainable. The experimental i_{Amal} obeys the behavior described by Myland and Oldham[66] (see eq 13 therein) for a mass-transport limited process at a sphere-cap type electrode. Furthermore, results extracted from COMSOL simulations agree with the experimental i_{Amal} and i_{Strip}. Additional experimental confirmation of these trends can be obtained from aqueous cadmium ASV data, which is presented as Supporting Information. Also, it is noteworthy that despite the possibility of forming diverse Li(Hg) phases,[40] the CV can be explained by a single reduction and stripping process occurring at approximately −1.67 V (vs CAR) over a wide concentration range.

Limit of Detection. The LOD for a method resulting in a linear calibration model of the form $y(x) = m{\cdot}x + b$ can be approximated by LOD = $3s_b/m$, where s_b is the standard error in the ordinate-intercept and m is the slope of the fit. The LODs based on this calculation are reported in Table 1. These results demonstrate that the detection of Li^+ can be performed over at least 2 orders of magnitude of concentration in PC and

dx.doi.org/10.1021/ac502517b | Anal. Chem. 2014, 86, 10660−10667

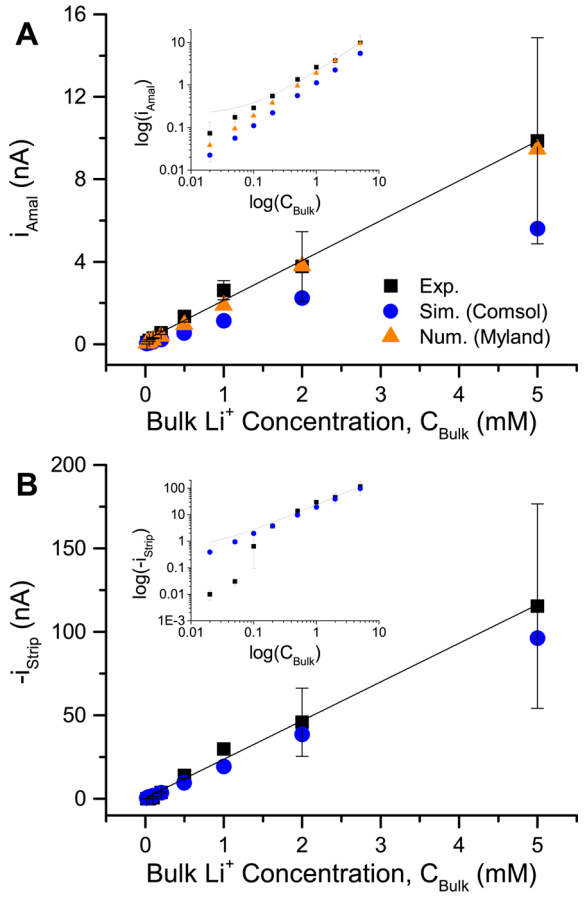

Figure 2. Calibration curves for the detection of Li^+ by the amalgamation current (A) and stripping peak current (B) at Hg/Pt UMEs. The error bars represent the standard deviation about the mean of six independent data sets and do not account for the 21% variance in the Hg cap volume.

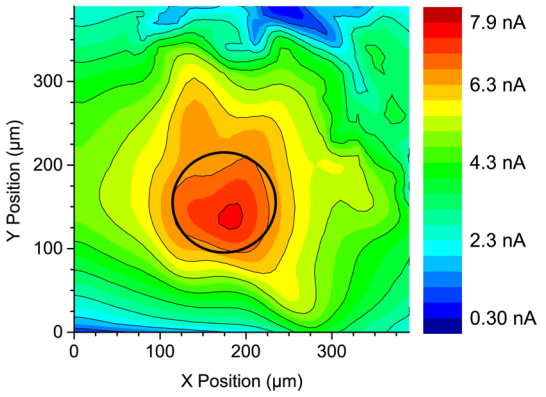

Figure 3. SECM image of a 120 μm diameter Au electrode (outlined in black) taken in SG-TC mode with ethyl viologen acting as the mediator. v_{Tip} = 10 μm/100 ms (100 μm·s^{-1}) and d_{Final} = 26.2 μm (2.3·r_{Pt}). An increase in redness indicates increased electrochemical activity at the substrate surface.

that good linearity is observed at concentrations below 5 mM. In individual concentration studies, Li^+ was detected down to 20 μM with a LOD as low as 19 μM by i_{Amal} and 28 μM by i_{Strip}. In comparison, the LOD from COMSOL simulations was 0.53 μM by i_{Amal} and 3.1 μM by i_{Strip}. This concentration range (19 μM to 5 mM) is well suited for recreating the main features of Li^+ intercalation and deposition processes.

Imaging of Reactivity. In order to test the *in situ* capabilities of Hg/Pt UMEs, competitive lithium stripping was performed in a battery-like environment, where lithium was electrodeposited on Au to mimic the uptake of lithium by battery electrodes during operation. The identification of an electroactive region (Figure 3) was facilitated by ethyl viologen's reduction at the Au substrate (E_{Subs} = −0.5 V) and regeneration at the Hg/Pt UME tip (E_{Tip} = +0.0 V). Once the SECM tip was aligned with an active portion of the Au substrate, the PTFE cell was rinsed twice with clean PC and then filled with 1 mM $LiClO_4$ in PC so that local changes in Li^+ concentration in response to substrate activation could be studied.

The amalgamation current at the Hg/Pt tip responded to electrochemical activity at the substrate. While positioned near the center of the 120 μm diameter electroactive Au spot (bold circle in Figures 3 and 5) and poised at −2.7 V (vs CAR), the Hg-capped probe reported i_{Amal} to be 1.18 nA, 0.50 nA, and −0.03 nA when the substrate CV reached +0.7 V, −0.8 V, and −3.0 V (vs CAR), respectively (Figure 4B). Thus, as the substrate was swept to greater overpotentials for lithium reduction, the tip collection current decreased in response. This relationship became the foundation of the imaging technique presented in this work.

Redox competition was exhibited not only in the tip collection current but also in the tip stripping current. A tip CV gave i_{Strip} as −2.79 nA, −1.51 nA, and −0.47 nA when the substrate was poised at +1.0 V, −0.8 V, and −3.0 V (vs CAR), respectively (Figure 4C). The stripping current provides solid confirmation that the electrochemical changes observe are due to the decrease in the local Li^+ concentration rather than presence of other additive cathodic processes, such as solvent decomposition.

Since the present system contained only one amalgam-forming species and because competing chemical processes did not constitute a significant portion of i_{Amal}, the chemical specificity afforded by fast scan CV or chronoamperometry was not necessary for this particular case. Therefore, the more accessible of the two parameters, the amalgamation current, was selected to investigate Li^+ flux.

Table 1. Linear Fits of Experimental and Simulated Li^+ Amalgamation and Stripping Behavior

signal, y	slope, m (pA·μM^{-1})	s_m	intercept, b (pA)	s_b	R^2	LOD (μM), 6 experiments	LOD (μM), 1 experiment
$i_{Amal, Exp.}$	1.93	0.058	191	112	0.9938	174.2	19[a]
$i_{Amal, Sim (COMSOL)}$	1.11744	5.3 × 10^{-5}	0.1	0.2	1		0.53
$i_{Amal, Num. (Myland)}$	1.89		0				
$-i_{Strip, Exp.}$	23.2	0.65	465	1272	0.9946	164.7	28[a]
$-i_{Strip, Sim. (COMSOL)}$	19.295	5.3 × 10^{-3}	−2	20	1		3.1

[a]Extrapolated from an analyte concentration range of 20 μM to 100 μM.

dx.doi.org/10.1021/ac502517b | *Anal. Chem.* 2014, 86, 10660−10667

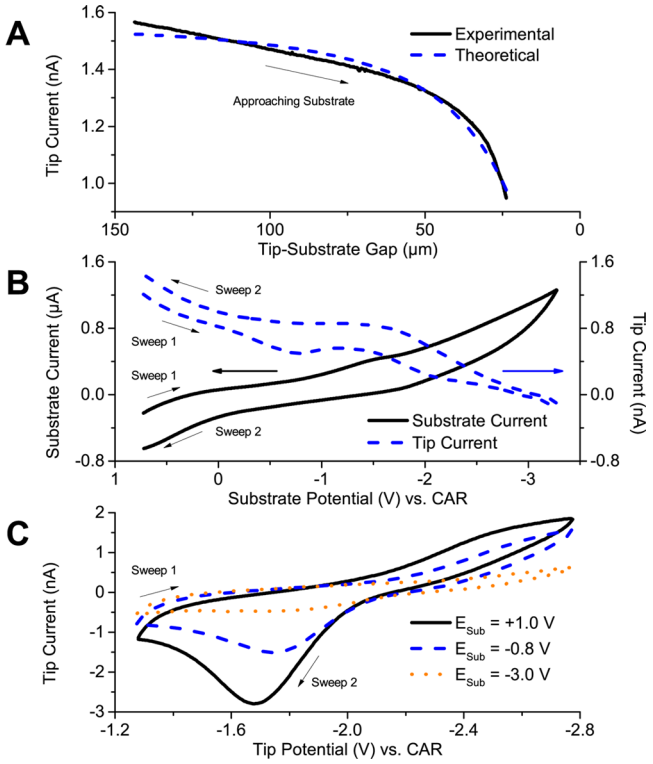

Figure 4. Detection of Li^+ fluxes in proximity to a 120 μm diameter Au electrode. (A) Probe approach curve at 200 nm/100 ms (2 $\mu m \cdot s^{-1}$). E_{Tip} = −2.7 V, E_{Subs} = Off, and d_{Final} = 23.8 μm (1.9·r_{Pt}). (B) Substrate CV, ν = 50 $mV \cdot s^{-1}$, E_{Tip} = −2.7 V. (C) Tip CVs, ν = 100 $mV \cdot s^{-1}$. All work was performed in PC containing 1 mM $LiClO_4$.

The amalgamation of lithium served as a reliable electrochemical process for monitoring the tip-to-substrate distance via negative feedback. An approach curve performed in 1 mM $LiClO_4$ in PC (Figure 4A) showed the characteristic decrease in Li^+ flux at the probe on nearing the substrate surface. The probe was positioned at a tip−substrate separation of 23.8 μm (1.9·r_{Pt}) based on fitting to an established mathematical model[60] for sphere-cap electrodes. Specific approach curve fitting parameters can be found in the Supporting Information (Table S-2). The ability to monitor the probe's position through the amalgamation of lithium makes Hg-capped electrodes practical for SECM in nonaqueous environments.

Spatial differences in Li^+ concentration are detectable by the Hg/Pt UME as differences in i_{Amal}. The central region of exposed electroactive Au substrate is not spatially resolved when biased at +1.0 V (vs CAR) (Figure 5A). Decreases in the tip current caused by impingement of the Hg cap by physically elevated features on the substrate revealed some PTFE debris, and overall the image shows only the effects of negative feedback. With the substrate biased at −0.8 V (vs CAR) (Figure 5B), the electroactive Au region remained indistinguishable from the surrounding PTFE-coated regions. However, the local Li^+ concentration decreased in response to the activation of the substrate electrode, thus establishing the sensitivity of the probe to the consumption of Li^+ by Au. Lastly, with the substrate biased at −3.0 V (vs CAR) (Figure 5C), the electroactive Au region became apparent as a circular region of low Li^+ concentration centered near [X = 175 μm, Y = 150 μm]. The conditions in Figure 5C were repeated with a slower tip velocity to emphasize the spatial heterogeneity in the Li^+ concentration gradient due to competition with the electroactive portion of the substrate. The resulting electrochemical map (Figure 5D) clearly indicates a Li^+-depleted region localized at the electroactive Au spot. The arc of low tip current from PTFE debris near [X = 200 μm, Y = 380 μm] continued to provide assurance that the substrate and Hg/Pt UME were in good alignment.

The tip current when passing over the electroactive spot was 1.84 nA, 0.81 nA, and 0.50 nA when the substrate was poised at +1.0 V, −0.8 V, and −3.0 V (vs CAR). Therefore, the substrate behaved as expected from substrate CVs (Figure 4B) when either fully deactivated or fully activated. Since the stationary and mobile currents agree, the mercury probe appears to be mechanically stable during lateral movement.

One possible shortcoming of continuously monitoring the i_{Amal} is that there is no way for lithium to leave the mercury phase during the imaging process. Chronoamperometric simulations in COMSOL (Figure S-9 in the Supporting Information) indicated that the 3.1 pL Hg sphere-cap used in Figure 5 reaches saturation within 193 s when biased at −2.7 V (vs CAR) in 1 mM $LiClO_4$. Since the data in Figure 5A−C were collected by rastering in 20 μm steps at 100 ms intervals (200 $\mu m \cdot s^{-1}$), the total Li^+ collection times were 82 s (accounting for the return scans). This translates into an internal lithium concentration of 396 mM or 44% of the solubility limit. This supports the notion that decreases in i_{Amal} used to create the electrochemical maps in Figure 5A−C were truly caused by depletion of surface-localized Li^+ due to uptake by the substrate and not merely spurious associations caused by saturation of the probe.

Interestingly, the high-resolution data set presented in Figure 5D was taken with ν_{Tip} = 10 μm/200 ms (50 $\mu m \cdot s^{-1}$). The collection time then was 642 s, which corresponds to 2.81 M lithium in the amalgam and exceeds the 898 mM lithium solubility limit. One possible explanation for the continued operation of the probe under such long collection times may be the formation of lithium-rich phases in the amalgam.[40] If so, this could help account for small shifts in the reduction potential and stripping peak shape under concentrated conditions (>2 mM $LiClO_4$) and slow scan rates (<50 $mV \cdot s^{-1}$). The probe's stability, then, is maximized under internally dilute conditions, achievable through fast scan rates and low bulk analyte concentrations. In order to facilitate high resolution, large area investigations, future work will aim to replace the constant potential imaging conditions with a fast scan CV approach, such as the one demonstrated by Alpuche-Aviles et al.[35] This will allow access to the selectivity information afforded by the stripping current and also prevent the saturation of the amalgam by lithium.

Nanostripping Experiments. It is desirable to increase the spatial resolution of the Hg-capped electrodes presented here. Ongoing work in the authors' laboratory aims to identify ideal conditions for reliably fabricating carbon-based nanoelectrodes (Figure S-10 in the Supporting Information). An example of Li^+ stripping at an Hg deposit on a 120 nm carbon electrode is shown in Figure 6. Integration of the Li stripping peak gives 5.48 pC, which corresponds to 52.9 amol Li in a 9 fL Hg drop (on the basis of the integration of the Hg deposition current). This amounts to 5.9 mM Li in the amalgam prior to stripping. This result demonstrates the feasibility of ASV at the nanoscale and suggests that amalgam saturation will not hamper SECM investigations based on the redox competition mode. We will soon employ these SECM probes to interrogate materials more

dx.doi.org/10.1021/ac502517b | Anal. Chem. 2014, 86, 10660−10667

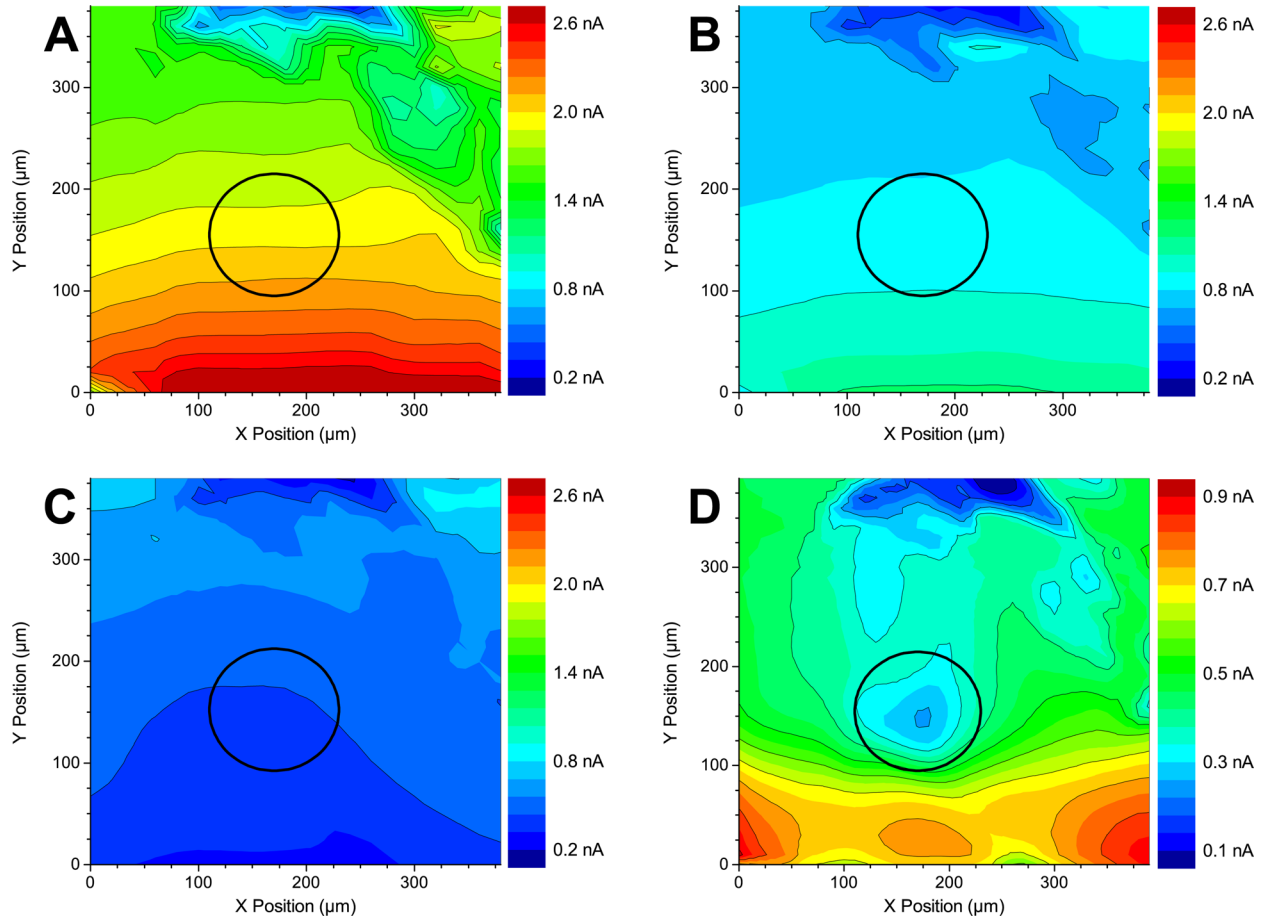

Figure 5. SECM images of Li^+ consumption using redox competition mode by an operating 120 μm diameter Au electrode (outlined in black). Lithium flux at the tip (E_{Tip} = −2.87 V) responded to differences in the substrate's activity toward lithium reduction when poised at +1.0 V (A), −0.8 V (B), and −3.0 V (C and D). Images A, B, and C were each acquired in 82 s with v_{Tip} = 20 μm/100 ms (200 μm·s^{-1}) and d_{Final} = 23.8 μm (1.9·r_{Pt}). Image D represents a higher resolution version of image C and was acquired in 642 s with v_{Tip} = 10 μm/200 ms (50 μm·s^{-1}). The probe was rastered in the *X*-direction. An increase in blueness indicates a decrease in free Li^+ concentration.

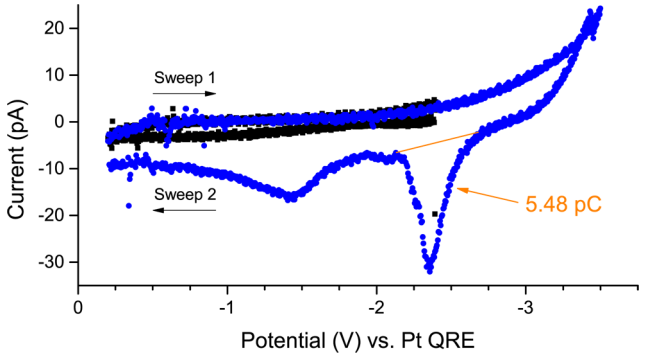

Figure 6. Lithium stripping at a mercury-capped carbon nanoelectrode, effective basal radius = 120 nm. Integration of the stripping peak marked by the orange baseline gives 5.48 pC. The potential was held at −3.2 V for 20 s in PC containing 1 mM $LiClO_4$.

recognizably applicable to energy storage and do so with reduced complications from diffusional broadening.

CONCLUSIONS

We have shown here for the first time the ability to electrochemically quantify lithium and other alkali ions in a nonaqueous medium for spatially resolved studies using SECM. Individual Hg/Pt UMEs have exhibited responses to as low as 20 μM Li^+ in PC with no additional time required to concentrate the amalgam beyond the ∼6 s spent sweeping the potential in CVs run at 100 mV·s^{-1}. The linear range of the probes, which extends over at least 2 orders of magnitude (20 μM Li^+ to 5 mM Li^+), permits their reliable operation in highly dynamic environments. Also, their 1.93 pA·μM^{-1} sensitivity of the amalgamation current to Li^+ ensures good resolution of differences in Li^+ flux. This is even more the case by the peak stripping current, which boasts a 23.2 pA·μM^{-1} sensitivity to ionic lithium. Furthermore, because of the chemical specificity of ASV, the possibility of quantifying Li^+ and other alkali ions simultaneously is well within reach.

Using PTFE-coated Au in PC as a proxy for electrode materials, Hg/Pt UMEs have identified surface features at the microscale by differences in the local Li^+ flux. Probe−substrate distance was monitored by the amalgamation of lithium at the tip, and approaches to the substrate were fit with an existing model for negative feedback at sphere-cap UMEs.[60] The agreement between stationary and mobile probe currents attests to their mechanical stability. The absence of substrate corrosion and the continued operation of the probe beyond the reported saturation concentration for lithium amalgams together confirm the chemical stability of the Hg-capped UMEs.

dx.doi.org/10.1021/ac502517b | *Anal. Chem.* 2014, 86, 10660−10667

Hg-based probes afford rapid, reliable, and robust quantification of alkali ions in conditions that are inaccessible to alternative approaches. A characterization of the sensitivity, useful range, and LOD for other s-block metals in organic media is forthcoming. Additionally, efforts to extend the application of Hg-capped probes to the nanoscale were introduced here and are an ongoing subject of study in our laboratory for a variety of energy material investigations.

■ ASSOCIATED CONTENT

Supporting Information

Electrochemical characterization data, cadmium stripping voltammograms, simulation parameters, and additional procedural details. This material is available free of charge via the Internet at http://pubs.acs.org.

■ AUTHOR INFORMATION

Corresponding Author

*E-mail: joaquinr@illinois.edu. Phone: (217) 300-7354. Fax: (217) 265-6290.

Author Contributions

Both authors have given approval to the final version of the manuscript.

Notes

The authors declare no competing financial interest.

■ ACKNOWLEDGMENTS

This material is based upon work supported by the National Science Foundation Graduate Research Fellowship Program under Grant No. DGE-1144245. Any opinions, findings, and conclusions or recommendations expressed in this material are those of the authors and do not necessarily reflect the views of the National Science Foundation. This work was also supported as part of the Joint Center for Energy Storage Research, an Energy Innovation Hub funded by the U.S. Department of Energy, Office of Science, Basic Energy Sciences. The authors also thank UIUC for generous start-up funds. The authors are grateful to Teresa C. Cristarella for assistance with preparing the insulated gold substrate, Dr. Mei Shen for valuable discussion, and Burton H. Simpson for the use of several carbon-based nanoelectrodes.

■ REFERENCES

(1) Bockris, J. O.'M.; Reddy, A. K. N. Electrochemistry. *Modern Electrochemistry 1: Ionics*, 2nd ed.; Plenum Press: New York, 1998; pp 1−34.

(2) Bockris, J. O.'M.; Reddy, A. K. N. Ion Transport in Solutions. In *Modern Electrochemistry 1: Ionics*, 2nd ed.; Plenum Press: New York, 1998; pp 361−600.

(3) Bard, A. J.; Faulkner, L. R. *Electrochemical Methods: Fundamentals and Applications*, 2nd ed.; Wiley: New York, 2001.

(4) Aurbach, D. *J. Power Sources* **2000**, *89*, 206−218.

(5) Verbrugge, M. W.; Koch, B. J. *J. Electrochem. Soc.* **2003**, *150*, A374−A384.

(6) Srinivasan, V.; Newman, J. *J. Electrochem. Soc.* **2004**, *151*, A1517−A1529.

(7) Goodenough, J. B.; Kim, Y. *Chem. Mater.* **2010**, *22*, 587−603.

(8) Harris, S. J.; Lu, P. *J. Phys. Chem. C* **2013**, *117*, 6481−6492.

(9) Wang, Y.; He, P.; Zhou, H. *Adv. Energy Mater.* **2012**, *2*, 770−779.

(10) Liu, J.; Zhang, J.-G.; Yang, Z.; Lemmon, J. P.; Imhoff, C.; Graff, G. L.; Li, L.; Hu, J.; Wang, C.; Xiao, J.; Xia, G.; Viswanathan, V. V.; Baskaran, S.; Sprenkle, V.; Li, X.; Shao, Y.; Schwenzer, B. *Adv. Funct. Mater.* **2012**, *23*, 929−946.

(11) Balke, N.; Jesse, S.; Kim, Y.; Adamczyk, L.; Tselev, A.; Ivanov, I. N.; Dudney, N. J.; Kalinin, S. V. *Nano Lett.* **2010**, *10*, 3420−3425.

(12) Lipson, A. L.; Ginder, R. S.; Hersam, M. C. *Adv. Mater.* **2011**, *23*, 5613−5617.

(13) Lipson, A. L.; Hersam, M. C. *J. Phys. Chem. C* **2013**, *117*, 7953−7963.

(14) Xu, F.; Beak, B.; Jung, C. *J. Solid State Electrochem.* **2011**, *16*, 305−311.

(15) Zampardi, G.; Ventosa, E.; La Mantia, F.; Schuhmann, W. *Chem. Commun.* **2013**, *49*, 9347−9349.

(16) Shao, Y.; Mirkin, M. V. *Anal. Chem.* **1998**, *70*, 3155−3161.

(17) Reymond, F.; Fermín, D.; Lee, H. J.; Girault, H. H. *Electrochim. Acta* **2000**, *45*, 2647−2662.

(18) Cousens, N. E. A.; Kucernak, A. R. *Electrochem. Commun.* **2011**, *13*, 1539−1541.

(19) Shen, M.; Ishimatsu, R.; Kim, J.; Amemiya, S. *J. Am. Chem. Soc.* **2012**, *134*, 9856−9859.

(20) Holtz, M. E.; Yu, Y.; Gunceler, D.; Gao, J.; Sundararaman, R.; Schwarz, K. A.; Arias, T. A.; Abruña, H. D.; Muller, D. A. *Nano Lett.* **2014**, *14*, 1453−1459.

(21) Bard, A. J.; Denuault, G.; Lee, C.; Mandler, D.; Wipf, D. O. *Acc. Chem. Res.* **1990**, *23*, 357−363.

(22) Eckhard, K.; Chen, X.; Turcu, F.; Schuhmann, W. *Phys. Chem. Chem. Phys.* **2006**, *8*, 5359−5365.

(23) Pust, S. E.; Maier, W.; Wittstock, G. *Z. Phys. Chem.* **2008**, *222*, 1463−1517.

(24) Bertoncello, P. *Energy Environ. Sci.* **2010**, *3*, 1620−1633.

(25) Mirkin, M. V.; Nogala, W.; Velmurugan, J.; Wang, Y. *Phys. Chem. Chem. Phys.* **2011**, *13*, 21196−21212.

(26) Rodríguez-López, J.; Zoski, C.; Bard, A. Application to Electrocatalysis and Photocatalysis and Surface Interrogation. In *Scanning Electrochemical Microscopy*, 2nd ed.; Bard, A. J., Mirkin, M. V., Eds.; CRC Press: Boca Raton, FL, 2012; Chapter 16, pp 525−568.

(27) Rodríguez-López, J.; Minguzzi, A.; Bard, A. J. *J. Phys. Chem. C* **2010**, *114*, 18645−18655.

(28) Tan, C.; Rodríguez-López, J.; Parks, J. J.; Ritzert, N. L.; Ralph, D. C.; Abruña, H. D. *ACS Nano* **2012**, *6*, 3070−3079.

(29) Ciani, I.; Daniele, S.; Bragato, C.; Baldo, M.-A. *Electrochem. Commun.* **2003**, *5*, 354−358.

(30) Daniele, S.; Baldo, M.-A.; Ugo, P.; Mazzocchin, G. A. *Anal. Chim. Acta* **1989**, *219*, 19−26.

(31) Nepomnyashchii, A. B.; Alpuche-Aviles, M. A.; Pan, S.; Zhan, D.; Fan, F.-R.; Bard, A. J. *J. Electroanal. Chem.* **2008**, *621*, 286−296.

(32) Selzer, Y.; Turyan, I.; Mandler, D. *J. Phys. Chem. B* **1999**, *103*, 1509−1517.

(33) Fernández, J. L.; Hurth, C.; Bard, A. J. *J. Phys. Chem. B* **2005**, *109*, 9532−9539.

(34) Souto, R. M.; González-García, Y.; Battistel, D.; Daniele, S. *Chem.—Eur. J.* **2011**, *18*, 230−236.

(35) Alpuche-Aviles, M. A.; Baur, J. E.; Wipf, D. O. *Anal. Chem.* **2008**, *80*, 3612−3621.

(36) Munteanu, G.; Munteanu, S.; Wipf, D. O. *J. Electroanal. Chem.* **2009**, *632*, 177−183.

(37) Hine, T. B. *J. Am. Chem. Soc.* **1917**, *39*, 882−895.

(38) Stevens, W. G.; Shain, I. *J. Phys. Chem.* **1966**, *70*, 2276−2280.

(39) Cogley, D. R.; Butler, J. N. *J. Phys. Chem.* **1968**, *72*, 1017−1020.

(40) Deiseroth, H.-J. *Prog. Solid State Chem.* **1997**, *25*, 73−123.

(41) Baranski, A.; Fawcett, W. R. *J. Chem. Soc., Faraday Trans. 1* **1980**, *76*, 1962−1977.

(42) Fawcett, W. R.; Baranski, A.; Drogowska, M. A. *J. Electroanal. Chem. Interfacial Electrochem.* **1986**, *215*, 237−247.

(43) Kwak, J.; Bard, A. J. *Anal. Chem.* **1989**, *61*, 1221−1227.

(44) Wipf, D. O.; Bard, A. J. *J. Electrochem. Soc.* **1991**, *138*, 469−474.

(45) Fan, F.-R.; Demaille, C. Preparation of Tips for Scanning Electrochemical Microscopy. In *Scanning Electrochemical Microscopy*, 2nd ed.; Bard, A. J., Mirkin, M. V., Eds.; CRC Press: Boca Raton, FL, 2012; Chapter 3, pp 25−52.

(46) Baldo, M.-A.; Daniele, S.; Mazzocchin, G. A. *Electrochim. Acta* **1996**, *41*, 811−818.

(47) Mauzeroll, J.; Hueske, E. A.; Bard, A. J. *Anal. Chem.* **2003**, *75*, 3880−3889.
(48) McNally, M.; Wong, D. K. Y. *Anal. Chem.* **2001**, *73*, 4793−4800.
(49) Singhal, R.; Bhattacharyya, S.; Orynbayeva, Z.; Vitol, E.; Friedman, G.; Gogotsi, Y. *Nanotechnology* **2009**, *21*, 015304.
(50) Velmurugan, J.; Mirkin, M. V. *Chem. Eur. J. Chem. Phys.* **2010**, *11*, 3011−3017.
(51) Morton, K. C.; Morris, C. A.; Derylo, M. A.; Thakar, R.; Baker, L. A. *Anal. Chem.* **2011**, *83*, 5447−5452.
(52) Takahashi, Y.; Shevchuk, A. I.; Novak, P.; Zhang, Y.; Ebejer, N.; Macpherson, J. V.; Unwin, P. R.; Pollard, A. J.; Roy, D.; Clifford, C. A.; Shiku, H.; Matsue, T.; Klenerman, D.; Korchev, Y. E. *Angew. Chem., Int. Ed.* **2011**, *50*, 9638−9642.
(53) Hu, K.; Gao, Y.; Wang, Y.; Yu, Y.; Zhao, X.; Rotenberg, S. A.; Gökmeşe, E.; Mirkin, M. V.; Friedman, G.; Gogotsi, Y. *J. Solid State Electrochem.* **2013**, *17*, 2971−2977.
(54) McKelvey, K.; Nadappuram, B. P.; Actis, P.; Takahashi, Y.; Korchev, Y. E.; Matsue, T.; Robinson, C.; Unwin, P. R. *Anal. Chem.* **2013**, *85*, 7519−7526.
(55) Marple, L. W. *Anal. Chem.* **1967**, *39*, 844−846.
(56) Manning, C. W.; Purdy, W. C. *Anal. Chim. Acta* **1970**, *51*, 124−126.
(57) Hall, J. L.; Jennings, P. W. *Anal. Chem.* **1976**, *48*, 2026−2027.
(58) Vieira, K. L.; Peters, D. G. *J. Electroanal. Chem. Interfacial Electrochem.* **1985**, *196*, 93−104.
(59) Rodríguez-López, J.; Alpuche-Aviles, M. A.; Bard, A. J. *Anal. Chem.* **2008**, *80*, 1813−1818.
(60) Lindsey, G.; Abercrombie, S.; Denuault, G.; Daniele, S.; De Faveri, E. *Anal. Chem.* **2007**, *79*, 2952−2956.
(61) Mussini, T.; Longhi, P.; Rondinini, S. *Pure Appl. Chem.* **1985**, *57*, 169−179.
(62) Cronnolly, C.; Pillai, K. C.; Waghorne, W. E. *J. Electroanal. Chem. Interfacial Electrochem.* **1986**, *207*, 177−187.
(63) Kozin, L. F.; Hansen, S. C. In *Mercury Handbook*; Royal Society of Chemistry: Cambridge, U.K., 2013; pp 50−60.
(64) Galus, Z. *Pure Appl. Chem.* **1984**, *56*, 635−644.
(65) Hills, G. J.; Peter, L. M. *J. Electroanal. Chem. Interfacial Electrochem.* **1974**, *50*, 175−185.
(66) Myland, J. C.; Oldham, K. B. *J. Electroanal. Chem. Interfacial Electrochem.* **1990**, *288*, 1−14.